Constraints on jet-driven disk accretion in Sagittarius A*

Erin J. D. Jolley and Zdenka Kuncic

School of Physics, University of Sydney, Sydney NSW, Australia

ABSTRACT

We revisit theoretical and observational constraints on geometrically-thin disk accretion in Sagittarius A* (Sgr A*). We show that the combined effects of mass outflows and electron energization in the hot part of the accretion flow can deflate the inflowing gas from a geometrically-thick structure. This allows the gas to cool and even thermalize on an inflow timescale. As a result, a compact, relatively cool disk may form at small radii. We show that magnetic coupling between the relativistic disk and a steady-state jet results in a disk that is less luminous than a standard relativistic disk accreting at the same rate. This relaxes the observational constraints on thin-disk accretion in Sgr A* (and by implication, other Low-Luminosity Active Galactic Nulcei, LLAGN). We find typical cold gas accretion rates of a few $\times 10^{-9} M_\odot \, \mathrm{yr}^{-1}$. We also find that the predicted modified disk emission is compatible with existing near-infrared (NIR) observations of Sgr A* in its quiescent state provided that the disk inclination angle is $\gtrsim 87°$ and that the jet extracts more than 75% of the accretion power.

Subject headings: Galaxy: nucleus - accretion - black hole physics - galaxies: jets - MHD

1. Introduction

The exceptionally compact radio source Sgr A* is spatially coincident with the dynamical centre of the Galaxy, which contains a mass $M \approx 3.7 \times 10^6 M_\odot$, deduced from measurements of stellar orbital motions (e.g. Ghez et al. 2000; Schödel et al. 2002; Eisenhauer et al. 2003). High-resolution VLBA imaging of Sgr A* at millimetre (mm) wavelengths provides the most compelling observational evidence yet for the existence of supermassive black holes (SMBHs), with M now constrained to lie within a radius $\approx 1 \, \mathrm{AU}$ of Sgr A* (Shen et al. 2005).

The observed bolometric luminosity of Sgr A*, $L \approx 10^{36} \, \mathrm{erg \, s}^{-1} \approx 2 \times 10^{-9} L_{\mathrm{Edd}}$ (where L_{Edd} is the Eddington luminosity), is unusually low, even compared to that of other LLAGN (Ho et al. 1997). This can be attributed to a very low mass accretion rate, $\dot{M}_{\mathrm{a}}$, or a low

radiative efficiency, $\epsilon = L/\dot{M}_\mathrm{a}c^2$, or to a combination of both. The most popular accretion models for Sgr A* are Radiatively Inefficient Accretion Flows (RIAFs), which have attributed the low L to a low ϵ and which are based on the hot ion torus (Shapiro, Lightman & Eardley 1976; Ichimaru 1977; Rees et al. 1982) and Advection Dominated Accretion Flow (ADAF; Narayan & Yi 1994) models.

Applications of RIAFs to Sgr A* have evolved considerably in recent years in response to increasing observational constraints (see Yuan 2006 for a review). In the original models, the inferred mass accretion rate was comparable to the Bondi rate for spherical accretion, $\simeq 10^{-5}\, M_\odot\, \mathrm{yr}^{-1}$, and the radiative efficiency was very low, $\epsilon \simeq$ a few $\times\, 10^{-6}$, as a result of preferential ion viscous heating and negligible electron-ion coupling. The most recent RIAF model (Yuan, Quataert & Narayan 2003, 2004) now takes into consideration a mass outflow component as well as energization of the electrons. As a result, the revised RIAF model now attributes the low luminosity of Sgr A* to a combination of low $\dot{M}_\mathrm{a}$ and moderately low ϵ. The outflow reduces the rate at which hot ionized gas is fed onto the central SMBH to levels that are consistent with mm and sub-mm polarization measurements, which require $\dot{M}_\mathrm{a} \lesssim 4 \times 10^{-8}\, M_\odot\, \mathrm{yr}^{-1}$ (Aitken et al. 2000; Agol 2000; Quataert & Gruzinov 2000; Bower et al. 2003; Marrone et al. 2006; Macquart et. al. 2006). Electron heating and acceleration are then required to produce the observed levels of radio and sub-mm emission (Quataert & Narayan 1999), resulting in a radiative efficiency $\epsilon \simeq 10^{-2}$.

The chanelling of binding energy away from the ions as a result of outflows and electron heating (as well as electron-ion coupling) necessarily implies that the ion energy is subvirial. There may then be insufficient ion pressure to support a geometrically-thick structure and consequently, some of the gas can radiatively cool on an inflow time (Rees et al. 1982). This raises the possibility that a compact, cool accretion disk may form at small radii. To test this possibility, the effects of a mass outflow on the continuity, angular momentum and energy equations need to be self-consistently considered in the exisiting RIAF model for Sgr A* (Yuan et al. 2003). Numerical approaches (e.g. Hawley & Balbus 2002; Sharma et al. 2007) have so far been limited by the nonconservative numerical scheme and the neglect of radiative cooling.

Observationally, increasing evidence is emerging to suggest that geometrically-thin disk accretion may persist at or near the last marginally stable orbit in low-luminosity sources (Miller et al. 2006a,b; Maoz 2007; Rykoff et al. 2007; Liu et al. 2007). Young massive stars seen orbiting the Galactic Center (GC) and believed to have formed *in situ* (Nayakshin & Sunyaev 2005; Nayakshin et al. 2006; Paumard et al. 2006; Nayakshin 2006; Levin et al. 2006; Beloborodov et al. 2006) suggest that at least some of the hot gas detected by *Chandra* has condensed into a cool phase. Additionally, new models for stellar wind accretion in Sgr A* indicate that slow

winds can radiatively cool within a dynamical timescale to produce a cold phase of accreting gas (Cuadra et al. 2006). However, a strong constraint on the presence of a cold, optically-thick disk is the absence of eclipses in the orbit of S2, the best studied star in the central S-cluster. This limits the size of a putative accretion disk to $\lesssim 10^{16}\,\mathrm{cm} \simeq 3 \times 10^5 r_\mathrm{g}$ (Cuadra, Nayakshin & Sunyaev 2003), where $r_\mathrm{g} = GM/c^2 \approx 5 \times 10^{11}(M/3.7 \times 10^6 M_\odot)\,\mathrm{cm}$ is the gravitational radius.

If a compact, cool disk forms near $\mathrm{Sgr\,A^\star}$, much of its emission would suffer strong interstellar extinction. Even so, the mass accretion rate would have to be extremely low and the spin axes of the disk and galactic plane would have to be closely aligned for the emission from a standard disk to remain below observational limits in the NIR (Cuadra et al. 2003; Trippe et al. 2007). However, it has been suggested (e.g. Nagar, Wilson & Falcke 2001; Falcke 2001; Falcke, Körding & Markoff 2004; Gallo 2007; Merloni & Heinz 2007) that the spectral properties of LLAGN and galactic X-ray binaries in their low/hard X-ray state can be attributed to a jet-dominated mode of accretion (see also Merloni & Fabian 2002). Although jets have not been observed in $\mathrm{Sgr\,A^\star}$, various arguments have been made for their presence (see e.g. Markoff, Bower & Falcke 2007, for a comprehensive discussion). If jets are present, an accretion disk can no longer be described by the standard model (Shakura & Sunyaev 1973; Novikov & Thorne 1973) because the radial disk structure is modified by the magnetic torque responsible for jet formation (Kuncic & Bicknell 2004, 2007b). Indeed, extraction of accretion power by a magnetized jet results in an accretion disk that is less luminous than a standard disk accreting at the same rate (Kuncic & Bicknell 2007a). That is, the radiative efficiency is lower than that predicted by standard accretion disk theory.

In this paper, we revisit theoretical constraints on the formation of a cool accretion disk and we investigate observational constraints on jet-driven disk accretion in $\mathrm{Sgr\,A^\star}$. Unlike the jet-RIAF model for $\mathrm{Sgr\,A^\star}$ (Falcke & Markoff 2000; Yuan, Markoff & Falcke 2002) and the disk-corona model for LLAGN (Merloni & Fabian 2002), we explicitly model the magnetic coupling between the accretion flow and the outflow. This model has been successfully applied to M87 (Jolley & Kuncic 2007). The organization of this paper is as follows. In Section 2, we show that a RIAF becomes geometrically-thin as a result of diversion of binding energy from the inflowing ions. This allows the electrons to radiatively cool and to thermalize with the ions on an inflow time, thus forming a cool disk at small radii. We also present the relevant equations for relativistic disk accretion modified by MHD stresses and we calculate the modified disk flux radial profile and corresponding modified disk emission spectrum using parameters appropriate for $\mathrm{Sgr\,A^\star}$. In Section 3, we calculate the steady-state synchrotron spectrum resulting from a jet magnetically coupled to the underlying accretion flow. We compare the predicted spectra with the observed quiescent spectrum for $\mathrm{Sgr\,A^\star}$.

A discussion and concluding remarks are given in Sections 4 and 5, respectively.

2. Coupling a Magnetized Jet to a Relativistic Disk

2.1. Formation of a Cool Disk

Weakly magnetized, differentially rotating accretion flows are unstable to MHD turbulence and electron heating is unavoidable as a result of viscous dissipation via a turbulent cascade as well as resistive dissipation via stochastic reconnection (Quataert & Gruzinov 1999; Bisnovatyi-Kogan & Lovelace 2000; Sano & Inutsuka 2001; Sharma et al. 2007). As the accretion flow becomes increasingly radiatively efficient, the internal energy of the ions drops to subvirial levels and the accretion flow geometry deflates from a geometrically-thick torus (Rees et al. 1982). If an outflow is also present, then this can further promote the collapse to a geometrically-thin structure, with a height-to-radius ratio $h/r \ll 1$.

To see this quantitatively, consider the internal energy equation for ions, with specific energy u_i, in an axisymmetric, steady and incompressible accretion flow with radial velocity v_r in which a fraction δ of the binding energy extracted by the internal MHD stresses $t_{r\phi}$ is diverted to the electrons and in which there is mass outflow with velocity v_z:

$$\frac{1}{r}\frac{\partial}{\partial r}\left(r\rho u_i v_r\right) + \frac{\partial}{\partial z}\left(\rho u_i v_z\right) = \frac{1}{2}t_{r\phi}\,r\frac{\partial \Omega}{\partial r} \tag{1}$$

Note that the current RIAF model (Yuan et al. 2003) neglects the outflow term involving v_z. Vertically integrating and using the relations $\dot{M}_a = 2\pi r\Sigma(-v_r)$ and $\partial \dot{M}_w/\partial r = -4\pi r\rho(h)v_z(h)$, where $\dot{M}_w$ is the mass loss rate and where continuity implies $\partial \dot{M}_a/\partial r = -\partial \dot{M}_w/\partial r$, gives

$$\frac{d}{dr}\left(\dot{M}_a u_i\right) + u_i\frac{d\dot{M}_w}{dr} = -2\pi r T_{r\phi}\,r\frac{\partial \Omega}{\partial r} \tag{2}$$

where $T_{r\phi}$ is the vertically-averaged stress. This is obtained from conservation of angular momentum:

$$-2\pi r T_{r\phi} = \dot{M}_a r\Omega\left[1 - \frac{\dot{M}_a(r_{\rm ms})}{\dot{M}_a(r)}\left(\frac{r}{r_{\rm ms}}\right)^{-1/2}\right] - \frac{1}{r}\int_{r_{\rm ms}}^{r} r^2\Omega\frac{d\dot{M}_a}{dr}\,dr \tag{3}$$

where $r_{\rm ms}$ is the last marginally stable orbit of the inflow. Substituting this into (2) to eliminate $T_{r\phi}$ and using $\dot{M}_a \propto r^s$ (Yuan et al. 2003), where $0 < s < 1$ and a keplerian angular velocity, $\Omega = (GM/r^3)^{1/2}$, yields the following solution for the ion internal energy:

$$u_i(r) = \frac{3}{2}\left[\frac{\frac{1}{2}(1-\delta)}{s+\frac{1}{2}}\right]\zeta(r)\frac{GM}{r} \tag{4}$$

where $\zeta(r) = 1 - (3/2 + s)^{-1}(r/r_{\mathrm{ms}})^{-1/2+s}$ is a small-r correction factor. This solution can be written in terms of the ion temperature T_{i} and the ion virial temperature $T_{\mathrm{vir,i}}$:

$$\frac{T_{\mathrm{i}}}{T_{\mathrm{vir,i}}} \approx \frac{\frac{1}{2}}{s + \frac{1}{2}}(1 - \delta) \tag{5}$$

Thus, the ions are subvirial. The current RIAF model for Sgr A* requires $\delta \gtrsim 0.5$ and numerical simulations (e.g. Hawley & Balbus 2002) indicate $s \approx 0.5 - 1$. Taking $s = 0.75$ for example, gives $T_{\mathrm{i}}/T_{\mathrm{vir,i}} \lesssim 0.2$.

This result has important implications for the radiative cooling and electron-ion collision rates, both of which are very sensitive to the scaleheight ratio $h/r \approx T_{\mathrm{i}}/T_{\mathrm{vir,i}}$ of an ion-pressure-supported disk. Consider the inflow timescale, $t^{\mathrm{inflow}} \simeq r/|v_r|$, and the bremsstrahlung cooling timescale (e.g. Rybicki & Lightman 1979),

$$t^{\mathrm{cool}} \simeq 7 \times 10^{10} n_{\mathrm{e}}^{-1} T_{\mathrm{e}}^{1/2}\ \mathrm{s} \tag{6}$$

where n_{e} is the electron number density (in units cm^{-3}) and T_{e} is the electron temperature (in K). Using $n_{\mathrm{e}} \approx \dot{M}_{\mathrm{a}}/(4\pi r \mu m_{\mathrm{p}} h|v_r|)$, the ratio of cooling to inflow timescales is

$$\frac{t^{\mathrm{cool}}}{t^{\mathrm{inflow}}} \simeq 100\, \frac{\epsilon}{\dot{m}}\, \frac{h}{r_{\mathrm{g}}}\, \frac{v_r^2}{c^2} \left(\frac{kT_{\mathrm{e}}}{m_{\mathrm{e}}c^2}\right)^{1/2} \tag{7}$$

where $\dot{m} \equiv \dot{M}_{\mathrm{a}}/\dot{M}_{\mathrm{Edd}}$ is the dimensionless mass accretion rate and $\dot{M}_{\mathrm{Edd}} = L_{\mathrm{Edd}}/(\epsilon c^2)$ is the Eddington accretion rate[1]. Using the relation $|v_r| = \frac{3}{2}\alpha c_{\mathrm{s}} \frac{h}{r}$ from the α-disk formalism, where $c_{\mathrm{s}} \approx (\gamma k T_{\mathrm{i}}/\mu m_{\mathrm{p}})^{1/2} = \Omega h$ is the isothermal sound speed, the condition $t^{\mathrm{cool}}/t^{\mathrm{inflow}} \lesssim 1$ required for the electrons to cool before reaching the black hole then implies (see also e.g. Rees et al. 1982)

$$\dot{m} \gtrsim 2 \times 10^{-9}\, \epsilon_{-2}\, \alpha_{-2}^2 \left(\frac{h}{0.1r}\right)^5 \left(\frac{kT_{\mathrm{e}}}{m_{\mathrm{e}}c^2}\right)^{1/2} \tag{8}$$

where $\epsilon_{-2} = \epsilon/10^{-2}$ and $\alpha_{-2} = \alpha/10^{-2}$. Typical values of α found in numerical simulations are a few percent (see Balbus 2003). Note that $\dot{m} = L/L_{\mathrm{Edd}} \approx 2 \times 10^{-9}$ for Sgr A*, implying that hot electrons with initial temperatures $T_{\mathrm{e}} \lesssim 10^{10}$ K can cool down by the time they reach the black hole.

If radiative cooling by bremsstrahlung emission resulting from electron-ion encounters can occur on an inflow time when the ions are subvirial, then it is necessary to also reconsider

---

[1]Note that we define $\dot{M}_{\mathrm{Edd}}$ without assuming a 10% radiative efficiency, as is done in RIAF models, in order to keep the dependence on ϵ explicit throughout the equations.

whether the Coulomb collision time can be shorter than the inflow time. The electron-ion collision time, $t^{\mathrm{ei}} \approx (\pi/2)^{1/2} m_{\mathrm{p}}/(m_{\mathrm{e}} n_{\mathrm{e}} \sigma_{\mathrm{T}} c \ln \Lambda)(kT_{\mathrm{e}}/m_{\mathrm{e}} c^2)^{3/2}$, can be written in terms of accretion parameters as

$$t^{\mathrm{ei}} \approx \left(\frac{\pi}{2}\right)^{1/2} \frac{1}{\ln \Lambda} \frac{\epsilon}{\dot{m}} \frac{h|v_r|}{c^2} \frac{m_{\mathrm{p}}}{m_{\mathrm{e}}} \frac{r}{r_{\mathrm{g}}} \left(\frac{kT_{\mathrm{e}}}{m_{\mathrm{e}} c^2}\right)^{3/2} \tag{9}$$

The condition $t^{\mathrm{ei}} \lesssim t^{\mathrm{inflow}}$ then requires

$$\dot{m} \gtrsim 50 \, \epsilon \, \alpha^2 \left(\frac{h}{r}\right)^5 \left(\frac{kT_{\mathrm{e}}}{m_{\mathrm{e}} c^2}\right)^{3/2} = 5 \times 10^{-10} \, \epsilon_{-2} \, \alpha_{-2}^2 \left(\frac{h}{0.1r}\right)^5 \left(\frac{kT_{\mathrm{e}}}{m_{\mathrm{e}} c^2}\right)^{3/2} \tag{10}$$

where a Coulomb logarithm $\ln \Lambda = 50$ has been used. Note that this differs from previous calculations (e.g. Rees et al. 1982) only in the explicit inclusion of h/r (previously taken as unity) and ϵ (previously taken as 0.1). For Sgr A*, with $\dot{m} \approx 2 \times 10^{-9}$, this implies electrons with temperatures $T_{\mathrm{e}} \lesssim 2 \times 10^{10}$ K can thermally couple with subvirial ions on an inflow time via Coulomb collisions. Note that collisionless wave-particle plasma microinstabilities can enhance the electron-ion coupling rate further (Begelman & Chiueh 1988; Quataert 1998; Gruzinov 1998; Quataert & Gruzinov 1999; Blackman 1999; Bisnovatyi-Kogan & Lovelace 2000; Melia et al. 2001).

As the disk cools, its scaleheight continues to decrease until the gas becomes optically thick. Initially, the opacity of the hot gas is dominated by electron scattering. The optical depth over the disk height is $\tau_{\mathrm{es}} \approx \sigma_{\mathrm{T}} \dot{M}_{\mathrm{a}}/(4\pi r \mu m_{\mathrm{p}} |v_r|)$, which exceeds unity when

$$\dot{M}_{\mathrm{a}} \gtrsim 7 \times 10^{-7} \alpha_{-2} \left(\frac{r}{100 r_{\mathrm{g}}}\right)^{1/2} \left(\frac{h}{0.1r}\right)^2 M_6 \, M_\odot \, \mathrm{yr}^{-1} \tag{11}$$

For Sgr A*, this implies a disk can become optically-thick once it collapses to scaleheights $h \lesssim$ a few $\times \, 10^{-3} r$. By then, however, the disk is sufficiently cool and dense that other opacities are more important than electron scattering, so the final disk height need not be too small.

We note that whilst numerical simulations (e.g. Sano & Inutsuka 2001; Sharma et al. 2007) demonstrate that preferential heating of electrons resulting from viscous and resistive turbulent dissipation occurs in low-$\dot{M}_{\mathrm{a}}$ accretion flows, they are yet to include radiative cooling in the calculations. This is needed in order to verify the above theoretical arguments. In the following, we assume that a cool, quasi-thermal disk has formed at small radii as a result of electron heating and mass outflows in the hot accretion flow at larger radii. A thermally-driven outflow is assumed to be negligible in the cool disk, but we consider the effects of a magnetically-driven outflow which we identify as a magnetized jet.

2.2. Magnetic Torque on the Disk Surface

The MHD stresses responsible for allowing accretion to proceed can give rise to a non-zero torque that acts over the disk surface, in addition to a non-zero torque at the last marginally stable orbit (Kuncic & Bicknell 2004). The effect of a non-zero magnetic torque acting on the surface of a relativistic disk has not been self-consistently modelled before. This torque does work against the disk surface, thereby removing energy from the disk and directing it vertically. Because it is associated with the azimuthal-vertical magnetic stress $t_{\phi z}^+ = B_\phi^+ B_z^+ / 4\pi$ at the disk surface (denoted by the '+' superscript), it can be identified with the formation of a magnetized corona and/or jet. Thus, the radiative flux from a relativistic, torqued disk can be most generally expressed as (see the Appendix for details)

$$F(r) = \frac{3GM\dot{M}_a}{8\pi r^3} \left[f^{\mathrm{NT}}(x) + f_{r\phi}^{\mathrm{nzt}}(x) - f_{\phi z}^{\mathrm{nzt}}(x) \right] \tag{12}$$

where $x = r/r_g$ is the dimensionless radius, $f^{\mathrm{NT}}(x)$ is the Novikov & Thorne (1973) relativistic correction factor, $f_{r\phi}^{\mathrm{nzt}}(x)$ is a correction factor for a nonzero torque (NZT) at the inner disk boundary (Agol & Krolik 2000), and $f_{\phi z}^{\mathrm{nzt}}(x)$ is an analogous correction factor for a nonzero torque on the disk surface. This is derived in Appendix A.2 and is explicitly given by

$$f_{\phi z}^{\mathrm{nzt}}(x) = \frac{4\pi r_g}{C(x)\dot{M}_a \Omega x^2} \int_{x_{\mathrm{ms}}}^x \frac{C^{1/2}}{B} t_{\phi z}^+ x^2 \, \mathrm{d}x \tag{13}$$

where $x_{\mathrm{ms}} = r_{\mathrm{ms}}/r_g$ is the dimensionless radius of the last marginally stable orbit and the dimensionless functions $C(x)$ and $B(x)$ are defined in the Appendix.

Henceforth, we consider a jet interpretation for the nonzero surface torque and assume a simple power law radial profile for the ϕz stress as follows (see also Freeland et. al. 2006):

$$t_{\phi z}^+(x) = t_{\phi z}^+(x_{\mathrm{ms}}) \left(\frac{x}{x_{\mathrm{ms}}} \right)^{-q} \tag{14}$$

The normalization of the nonzero MHD stresses $t_{\phi z}^+(x_{\mathrm{ms}})$ and $T_{r\phi}(x_{\mathrm{ms}})$ are yet to be determined. We now achieve this by considering the global constraint imposed by energy conservation.

2.3. The Global Energy Budget

Global energy conservation requires that the total accretion power P_a must equal the sum of the disk radiative power L_d and the jet power P_j, which we equate to the rate at

which work is done against the disk by the nonzero magnetic torque on its surface. Hence,

$$P_{\mathrm{a}} = L_{\mathrm{d}} + P_{\mathrm{j}} \tag{15}$$

We now write

$$
\begin{aligned}
P_{\mathrm{a}} &= \epsilon_{\mathrm{a}} \dot{M}_{\mathrm{a}} c^2 = \left(\epsilon^{\mathrm{NT}} + \Delta\epsilon\right) \dot{M}_{\mathrm{a}} c^2 \\
P_{\mathrm{j}} &= \epsilon_{\mathrm{j}} \dot{M}_{\mathrm{a}} c^2
\end{aligned}
\tag{16}
$$

where $\epsilon_{\mathrm{a}} = \epsilon^{\mathrm{NT}} + \Delta\epsilon$ is the total accretion efficiency and ϵ_{j} is the efficiency of energy removal to a jet. The efficiencies are defined as follows:

$$\epsilon^{\mathrm{NT}} = \frac{3}{2} \int_{x_{\mathrm{ms}}}^{\infty} x^{-2} f^{\mathrm{NT}}(x)\, \mathrm{d}x = \frac{3}{2} \int_{x_{\mathrm{ms}}}^{\infty} x^{-2} \frac{A(x)}{C(x)}\, \mathrm{d}x \tag{17}$$

$$\Delta\epsilon = \frac{3}{2} \int_{x_{\mathrm{ms}}}^{\infty} x^{-2} f_{r\phi}^{\mathrm{nzt}}(x)\, \mathrm{d}x = \frac{C_{\mathrm{ms}}^{1/2}}{B_{\mathrm{ms}}} \frac{3\pi x_{\mathrm{ms}}^2 T_{r\phi}(x_{\mathrm{ms}}) r_{\mathrm{g}}}{\dot{M}_{\mathrm{a}} c} I_3 \tag{18}$$

$$\epsilon_{\mathrm{j}} = \frac{3}{2} \int_{x_{\mathrm{ms}}}^{\infty} x^{-2} f_{\phi z}^{\mathrm{nzt}}(x)\, \mathrm{d}x = \frac{6\pi x_{\mathrm{ms}}^q r_{\mathrm{g}}^2 t_{\phi z}^{+}(x_{\mathrm{ms}})}{\dot{M}_{\mathrm{a}} c} I_2 \tag{19}$$

where

$$I_1(x) = \int_{x_{\mathrm{ms}}}^{x} \frac{[C(x)]^{1/2}}{B(x)} x^{2-q}\, \mathrm{d}x \tag{20}$$

$$I_2 = \int_{x_{\mathrm{ms}}}^{\infty} \frac{x^{-5/2}}{C(x)} I_1(x)\, \mathrm{d}x \tag{21}$$

$$I_3 = \int_{x_{\mathrm{ms}}}^{\infty} \frac{x^{-5/2}}{C(x)}\, \mathrm{d}x \tag{22}$$

Thus, the nonzero torques can be normalized in terms of the corresponding efficiencies $\Delta\epsilon$ and ϵ_{j} and the terms $f_{r\phi}^{\mathrm{nzt}}(x)$ and $f_{\phi z}^{\mathrm{nzt}}(x)$ can be rewritten as follows:

$$f_{r\phi}^{\mathrm{nzt}}(x) = \frac{2}{3} \frac{\Delta\epsilon}{C(x) x^{1/2} I_3} \tag{23}$$

$$f_{\phi z}^{\mathrm{nzt}}(x) = \frac{2}{3} \frac{\epsilon_{\mathrm{j}}}{C(x) x^{1/2}} \frac{I_1(x)}{I_2} \tag{24}$$
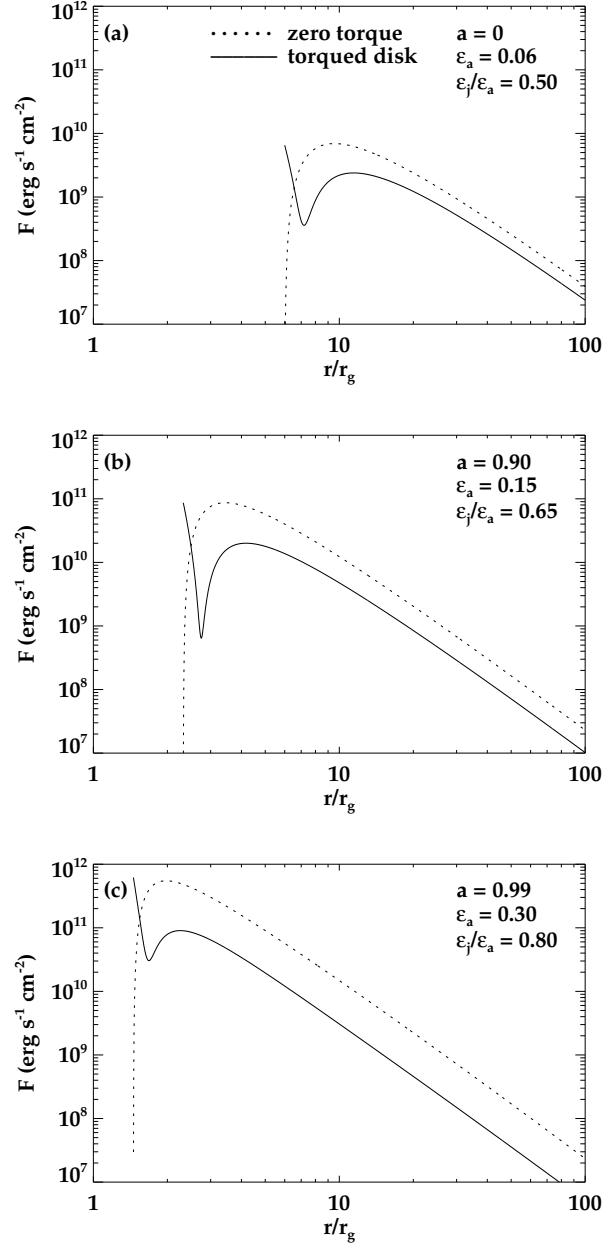
Fig. 1.— Radial flux profiles for the jet-modified disk model (solid curves) with different physical parameters: a is the dimensionless black hole spin parameter; ϵ_a is the overall accretion efficiency, which includes a fractional contribution of 5% of the Novikov-Thorne efficiency resulting from a nonzero torque at the last marginally stable orbit r_{ms}; and ϵ_j/ϵ_a is the fractional power removed by a surface magnetic torque responsible for jet formation. The disk luminosity is $L_d = 10^{-8} L_{Edd} \approx 5 \times 10^{36} \mathrm{erg\,s}^{-1}$ in all cases. The dotted curves show the corresponding radial flux profiles for a standard, non-torqued relativistic disk.

2.4. The Modified Disk Flux Radial Profile and Spectrum

We now substitute the above expressions into the disk flux profile (12):

$$F(r) = \frac{3GM\dot{M}_{\rm a}}{8\pi r^3} \left[\frac{A(x)}{C(x)} + \frac{2}{3}\frac{\Delta\epsilon}{C(x)x^{1/2}I_3} - \frac{2}{3}\frac{\epsilon_{\rm j}}{C(x)x^{1/2}}\frac{I_1(x)}{I_2} \right] \tag{25}$$

The global energy constraint (15) yields the following for the disk radiative efficiency:

$$\epsilon_{\rm d} = (\epsilon^{\rm NT} + \Delta\epsilon)\left(1 - \frac{\epsilon_{\rm j}}{\epsilon_{\rm a}}\right) \tag{26}$$

We can also write

$$\dot{M}_{\rm a} = \left(\frac{L_{\rm d}}{L_{\rm Edd}}\right)\frac{L_{\rm Edd}}{\epsilon_{\rm d}c^2} \tag{27}$$

where $L_{\rm Edd} = 4\pi GM m_{\rm p}c/\sigma_{\rm T} \approx 1.3 \times 10^{44}M_6\,{\rm erg\,s^{-1}}$. Thus, once $\Delta\epsilon$ and $\epsilon_{\rm j}/\epsilon_{\rm a}$ are specified (and note that $\epsilon^{\rm NT}$ is given explicitly by (17) and depends only on the dimensionless spin parameter a), we have determined $\epsilon_{\rm d}$. Then the mass accretion rate is determined by specifying $L_{\rm d}/L_{\rm Edd}$ and using (27). The fraction $\epsilon_{\rm j}/\epsilon_{\rm a}$ of accretion power injected into a jet cannot be arbitrarily large, however, since the local disk flux must remain positive at all radii. So for a given set of input parameters, a, $\Delta\epsilon/\epsilon^{\rm NT}$, and $L_{\rm d}/L_{\rm Edd}$, there is a maximum allowable value of $\epsilon_{\rm j}/\epsilon_{\rm a}$.

The radial flux profiles predicted by our torqued relativistic disk model (c.f. (25)) are shown in Figure 1 (solid curves). In all cases, the rate of radial decline in the surface magnetic stresses is fixed at $q = 2.5$ (c.f. (14)). The efficiency of energy dissipation by the magnetic torque at the inner boundary is set to $\Delta\epsilon = 0.05\epsilon^{\rm NT}$. The intrinsic luminosity of the modified disk is $L_{\rm d} = 10^{-8}L_{\rm Edd} \approx 5 \times 10^{36}\,{\rm erg\,s^{-1}}$ in all cases. The flux profiles are calculated for a range of black hole spin parameters a and fractional jet powers $\epsilon_{\rm j}/\epsilon_{\rm a}$, as indicated in each plot. Note that as a, and therefore $\epsilon_{\rm a}$, increase, a larger fraction $\epsilon_{\rm j}/\epsilon_{\rm a}$ of the accretion power must be electromagnetically extracted to maintain a constant $L_{\rm d}$. The mass accretion rates are as follows: (a) $\dot{M}_{\rm a} \approx 3 \times 10^{-9}M_\odot\,{\rm yr^{-1}}$, (b) $\dot{M}_{\rm a} \approx 1 \times 10^{-9}M_\odot\,{\rm yr^{-1}}$ and (c) $\dot{M}_{\rm a} \approx 1 \times 10^{-9}M_\odot\,{\rm yr^{-1}}$. The corresponding profiles for a non-torqued disk (dotted curves) are calculated using the same values of $\dot{M}_{\rm a}$, but in that case, $\epsilon_{\rm d} \approx \epsilon_{\rm a}$ because all the accretion power is dissipated locally in the disk.

The effect of the nonzero torque across the disk surface is to do work against the disk, thus reducing the disk flux over the range of radii where the magnetic torque is strongest. This counteracts the effect of the nonzero torque at the inner disk boundary, which enchances the disk flux near $x_{\rm ms}$. The combined effects of these two torques is clearly evident in the radial flux profiles in Fig. 1 (solid curves). The resulting radial profiles are substantially

modified from their corresponding zero-torque profiles (Fig. 1, dotted lines). It is clear from Fig. 1 that the nonzero magnetic torque acting on the disk surface results in a disk radiative efficiency ϵ_d that is lower than that of a non-torqued disk.

Figure 2 shows the disk spectra corresponding to the flux profiles in Fig. 1. The spectra have been calculated assuming local blackbody emission in each annulus of the disk, with the local temperature determined by $T(r) = [F(r)/\sigma]^{1/4}$, where $F(r)$ is given by (25) and σ is the Stefan-Boltzmann constant. We have included a $\cos\theta_\mathrm{d}$ projection factor, where θ_d is the angle between the disk spin axis and our line of sight. Note that in all cases, the effect of the MHD torque on the disk surface is to make the emergent spectrum (solid curves) dimmer and redder than that of a non-torqued disk accreting at the same rate (dotted curves). The effect is strongest for the high spin case (Fig. 2c) because the overall accretion efficiency is highest in that case and to maintain the same L_d, the jet must remove a larger fraction of the total accretion power.

3. Jet Synchrotron Emission

We identify the nonzero magnetic torque across the disk surface with the mechanism responsible for extracting accretion power from the disk and injecting it directly into a jet. This torque could also produce a magnetized coronal outflow, in which case only a fraction of the extracted power may result in a jet (see e.g. Merloni & Fabian 2002). Some of the magnetic energy is subsequently converted into kinetic energy. We expect a fraction of the particles to be accelerated to nonthermal, relativistic energies. Synchrotron radiation by relativistic electrons will then contribute significantly to the radio emission. It has been proposed (Falcke & Markoff 2000) that highly efficient acceleration of electrons and synchrotron emission at the base of the jet may explain the observed sub-mm excess emission from Sgr A*.

3.1. The Jet Model

We divide the jet into a series of quasi-cylindrical sections of thickness Δz, and calculate the total emission spectrum by summing the contributions from each component. The geometry is illustrated in Figure 3.

The jet plasma is assumed to have a magnetic field strength B and to contain nonthermal electrons, with Lorentz factors in the range $\gamma_\mathrm{min} \leq \gamma \leq \gamma_\mathrm{max}$, where γ_min and γ_max are the minimum and maximum electron Lorentz factors respectively. The nonthermal electron
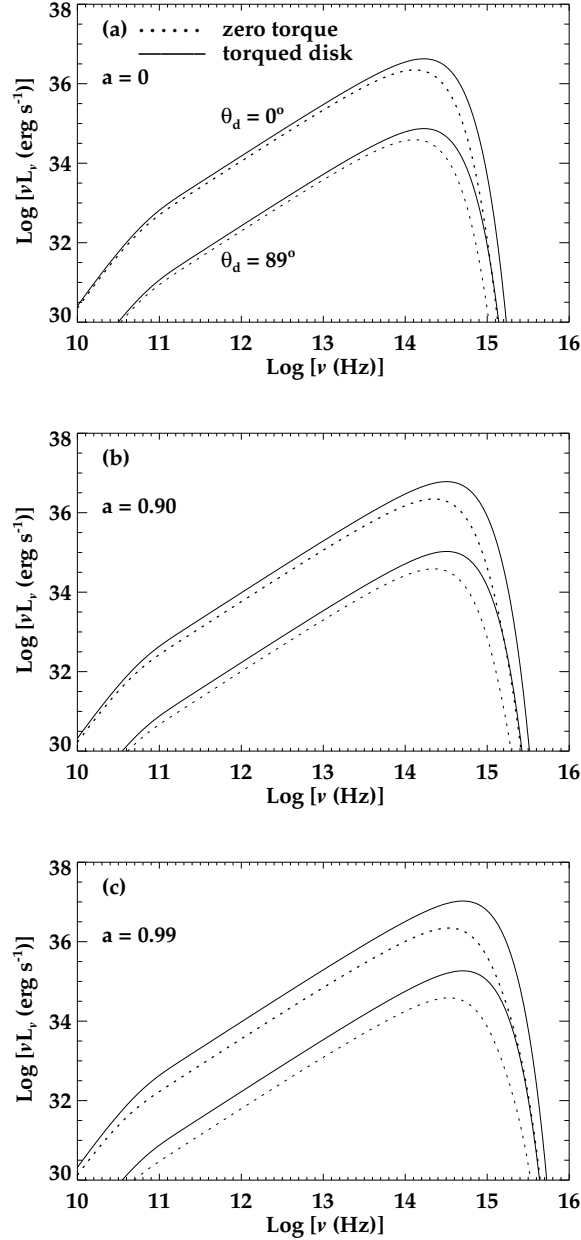
Fig. 2.— Predicted disk spectra for the jet-modified disk model. The dimensionless black hole spin parameter a is and θ_{d} is the inclination angle of the disk. All other model parameters are the same as those used in the corresponding flux profiles shown in Fig. 1. The solid curves are the predicted spectra for a relativistic disk torqued at the inner boundary and on its surface; the dotted curves are spectra for a non-torqued relativistic disk (i.e. a Novikov-Thorne disk). In each plot, the upper two curves are for a disk oriented face-on ($\theta_{\mathrm{d}} = 0$) and the lower two curves are for a disk oriented nearly egde-on ($\theta_{\mathrm{d}} = 89°$).
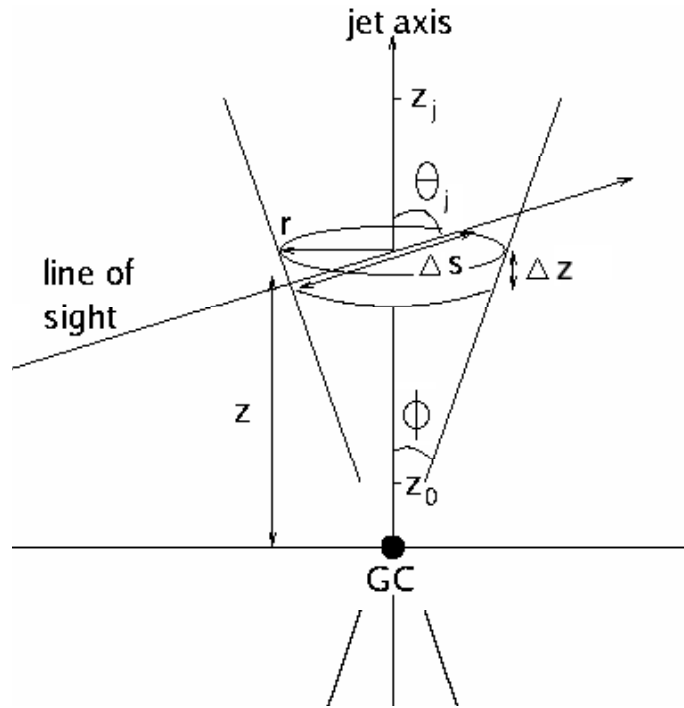
Fig. 3.— Schematic diagram of the jet geometry (not to scale). The jet begins at a height z_0 and extends to z_j, with half opening angle ϕ. It is divided into cylindrical sections of thickness Δz and radius $r \approx z\phi$. The angle between the jet axis and the line of sight is θ_j and the path length through each cylinder is Δs. The distance to the galactic centre is $D_{GC} \approx 8.5\,\mathrm{kpc}$.

energy distribution is given by $N_e(\gamma) \propto \gamma^{-p}$ where $N_e = \int N_e(\gamma)\, d\gamma$ is the total electron number density.

We consider a relativistic jet with bulk Lorentz factor Γ_j, half-opening angle $\phi \approx 1/\Gamma_j$, and Doppler factor

$$\delta = \left\{ \Gamma_j \left[1 - (1 - \Gamma_j^{-2})^{1/2} \cos\theta_j \right] \right\}^{-1} \qquad , \tag{28}$$

where θ_j is the angle between our line of sight and the jet axis (see Fig. 3). We use the following simple radiative transfer model to calculate the observed specific luminosity due to the net contribution from each jet component (assuming isotropic emission in the source rest frame):

$$L_{\nu_{obs}}^{obs} \approx 2 \sum_{z=z_0}^{z_j} 4\pi \delta^3 S_{\nu_{obs}}^{syn} \left(1 - e^{-\tau_{\nu_{obs}}^{syn}} \right) \Delta A \tag{29}$$

where $\Delta A \approx \pi r \Delta z \sin\theta$ is the projected surface area of each emitting cylinder, $S_{\nu_{obs}}^{syn}$ is the synchrotron source function (see e.g. Rybicki & Lightman 1979 for relevant formulas) and

$$\tau_{\nu_{obs}}^{syn} = \delta^{-1} \kappa_{\nu_{obs}}^{syn} \Delta s$$

is the synchrotron optical depth along a path length $\Delta s \approx 2r/\cos\theta_j$, where $r \approx z\phi$ through each section.

We use an equipartition factor $f_{eq} = U_B/U_e$ to relate the magnetic field energy density $U_B = B^2/8\pi$ directly to the relativistic electron energy density $U_e = \frac{4}{3}\langle\gamma\rangle N_e m_e c^2$, where $\langle\gamma\rangle$ is the average Lorentz factor. The electron number density N_e and hence the magnetic field B decline with jet height z according to

$$N_e(z) \propto z^{-2} \qquad , \qquad B(z) \propto z^{-1}$$

The total jet power is

$$\begin{aligned} P_j \quad &\approx \pi r_j^2 \Gamma_j (1 - \Gamma_j^{-2})^{1/2} c \times \\ &\left[(\Gamma_j - 1) N_e m_p c^2 + \frac{4}{3} \Gamma_j N_e \langle\gamma\rangle m_e c^2 \left(1 + 2 f_{eq} \right) \right] \end{aligned} \tag{30}$$

where the first term in square brackets refers to the bulk jet kinetic energy and the second term refers to the electron kinetic energy and the magnetic energy. This is used to normalize the electron number density $N_{e,0}$ at the base of the jet once the ratio ϵ_j/ϵ_a (or equivalently P_j/P_a) is specified.

3.2. Application to Sgr A*

Figure 4 shows the best-fit broadband spectra predicted by our magnetically coupled disk-jet model plotted against data points for observations of Sgr A* in quiescence (compiled by Narayan et al. 1998; Falcke et al. 1998; Broderick & Narayan 2006). The best-fit disk parameters are listed in Table 1. The disk inclination angle is $\theta_d = 87°$ in both the zero-spin and high-spin cases. We generally find that the jet needs to extract the maximum fraction ϵ_j/ϵ_a of accretion power from the disk to produce an energetically significant spectral component in the sub-mm. For the jet spectrum, we used $\theta_j = 55°$ (Falcke & Markoff 2000) and we found that a total jet length of just $z_j \approx 350 r_g \simeq 6 \times 10^{-5}$ pc was needed to fit the lowest radio frequency data points (this corresponds to an angular size of $\theta \simeq 1.5$ mas at the distance to Sgr A*). The jet is launched from an initial height $z_0 = 0.1 r_{ms}$ above the disk midplane, where $r_{ms} = 6 r_g$ for $a = 0$ and $r_{ms} = 1.5 r_g$ for $a = 0.99$. The electron energy power-law index is $p = 1.9$. The other jet input parameters used are as follows: (a) ($a = 0$ case) $\Gamma_j = 1.05$, $f_{eq} = 30$, $\gamma_{min} = 30$, $\gamma_{max} = 150$; and (b) ($a = 0.99$ case) $\Gamma_j = 1.9$, $f_{eq} = 1$, $\gamma_{min} = 50$, $\gamma_{max} = 100$. The corresponding electron number density and magnetic field strength at the base of the jet are: (a) $N_{e,0} \approx 1 \times 10^6$ cm^{-3}, $B_0 \approx 230$ G; and (b) $N_{e,0} \approx 1 \times 10^8$ cm^{-3}, $B_0 \approx 430$ G. Despite the large difference in $N_{e,0}$, the predicted jet spectra for the two cases are remarkably similar. This is because the lower $N_{e,0}$ for the $a = 0$ case is offset by the larger length scale, since we set $z_0 = 0.1 r_{ms}$ in both cases and r_{ms} is larger by a factor of 4 for the $a = 0$ case. The location of the synchrotron self-absorption turnover is sensitive to the value of $N_{e,0}$ and we find that $z_0 = 0.1 r_{ms}$ gives a turnover in the sub-mm in both cases, which is suggested by the observations.

Note that in both the $a = 0$ and $a = 0.99$ cases, we find that a relatively narrow range of electron Lorentz factors, $\gamma_{min} \lesssim \gamma \lesssim \gamma_{max}$, is required to produce a prominent "bump" feature in the sub-mm. The range of electron energies is not sufficiently wide to produce a broadband optically-thin synchrotron power-law spectrum, so the spectrum cuts off sharply above the maximum critical frequency at the base of the jet, $\sim 4 \times 10^6 \gamma_{max}^2 B$ Hz. A similar requirement was also found by Falcke & Markoff (2000) for their RIAF-jet model. We find it difficult to fit the peak in the sub-mm excess feature at frequencies $\gtrsim 100$ GHz. It is likely that one or more of our simplifying assumptions (e.g. keeping γ_{min} and γ_{max} constant throughout the jet) may need to be relaxed in order to test more thoroughly the jet interpretation of the sub-mm excess. However, the observational data are mostly upper limits in this band and there may be other contributions to this spectral component, such as warm dust emission (e.g. Becklin et al. 1982).

The main difference between the high-spin and low-spin disk-jet models is that the $a = 0.99$ model predicts a larger jet kinetic power and a bluer disk spectrum compared to

Table 1: Disk parameters used in the coupled disk-jet spectral model shown in Figure 4. The dimensionless black hole spin is a, ϵ_j/ϵ_a is the fraction of accretion power extracted by the magnetized jet, ϵ_a is the total accretion efficiency, ϵ_d is the disk radiative efficiency, $\dot{M}_a$ is the mass accretion rate in $M_\odot\,\mathrm{yr}^{-1}$ and P_j is the jet power in $\mathrm{erg\,s}^{-1}$. The black hole mass is fixed at $M = 3.7 \times 10^6 M_\odot$ and the total disk luminosity is fixed at $L_d = 10^{-8} L_{\mathrm{Edd}} \approx 5 \times 10^{36} \mathrm{erg\,s}^{-1}$.

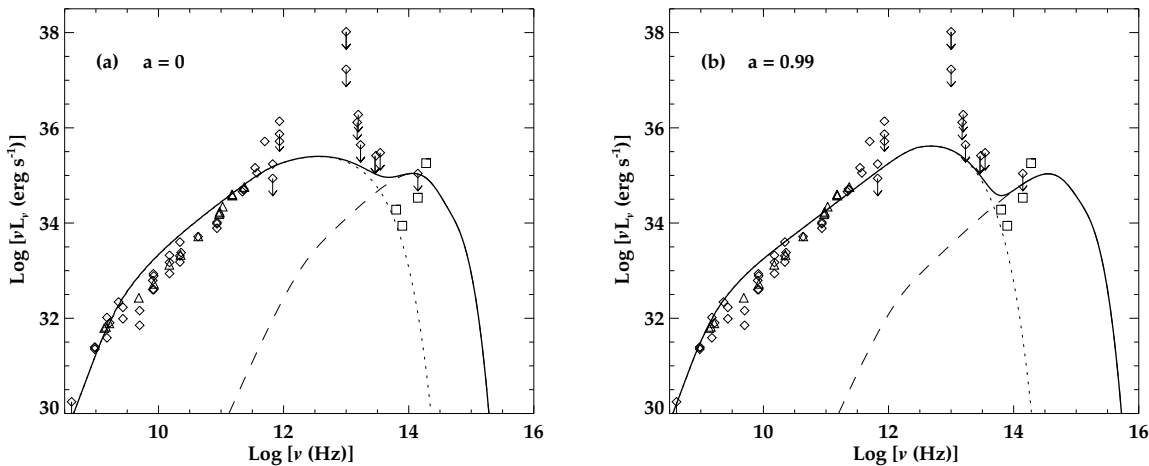| input parameters			inferred parameters		
a	ϵ_j/ϵ_a	ϵ_a	ϵ_d	$\dot{M}_a$	P_j
0.00	0.75	0.06	0.02	5×10^{-9}	1×10^{37}
0.99	0.90	0.31	0.03	3×10^{-9}	5×10^{37}

Fig. 4.— Broadband steady-state spectra predicted by the magnetically coupled disk-jet model for (a) a zero-spin black hole and (b) a high-spin black hole, compared against dereddened observations of Sgr A* in quiescence. The solid line is the total disk+jet spectrum predicted by our model, the dotted line is the jet synchrotron spectrum and the dashed line is the modified disk spectrum for an inclination of $\theta_d = 87°$. The diamonds, triangles and squares are data points compiled by Narayan et al. (1998), Falcke et al. (1998) and Broderick & Narayan (2006), respectively.

the $a = 0$ model. The larger jet kinetic power for the $a = 0.99$ model arises because a spinning black hole can extract more accretion power P_a than a non-spinning hole accreting at the same rate (and note in Table 1 that the accretion rate for the $a = 0.99$ model is only slightly lower than that for the $a = 0$ model, whereas the accretion efficiency is more than a factor of 4 higher). A bluer disk spectrum is predicted by the $a = 0.99$ model because the accretion disk extends all the way down to a last marginally stable orbit of $r_{\rm ms} \approx 1.5 r_{\rm g}$ (compared to $r_{\rm ms} \approx 6 r_{\rm g}$ for the $a = 0$ model) and thus, the peak temperature of the accretion disk is higher in the high-spin case than in the low-spin case. For an intrinsic disk luminosity $L_{\rm d} \approx 5 \times 10^{36} \, {\rm erg \, s^{-1}}$, we find $\theta_{\rm d} \gtrsim 87°$ (i.e. the disk is almost edge-on) is required for the disk spectrum to fall below the observational upper limit in the near infra-red (see Fig. 4). Importantly, this data point places an even stronger observational constraint on a standard accretion disk model, which predicts a higher $L_{\rm d}$ and therefore requires an even higher $\theta_{\rm d}$ for the same $\dot{M}_{\rm a}$. This is because a standard disk model predicts that all the accretion power is radiated by the disk, whereas our jet-modified disk model takes into account magnetic extraction of accretion power by a jet and hence, predicts a dimmer and redder disk compared to that of a standard disk accreting at the same rate.

4. Discussion

We have demonstrated that the low radiative output from Sgr A* is not incompatible with a slowly accreting, geometrically thin cool disk. We have suggested that such a disk may form at small radii as a result of mass outflows and electron heating in the hot part of the accretion flow. These effects divert binding energy from the ions, thus reducing the scaleheight, allowing radiative cooling and Coulomb collisions to operate on an inflow time. Numerical simulations of low-$\dot{M}_{\rm a}$ accretion flows that include radiative cooling are needed to test this prediction. We infer cold gas accretion rates of $\dot{M}_{\rm a} \simeq$ a few $\times \, 10^{-9} {\rm M_\odot \, yr^{-1}}$. The disk radiative efficiency, $\epsilon_{\rm d} \approx 0.02 - 0.03$, is lower than the total accretion efficiency $\epsilon_{\rm a}$ because accretion power is extracted from the disk to form a jet.

An important observational test of this model is the predicted disk luminosity, which is difficult to constrain observationally owing to the nearly edge-on orientation of the disk (Trippe et al. 2007) and strong ($\sim 30 \, {\rm mag}$) interstellar extinction (see e.g. Cuadra et al. 2003). We have shown here that an intrinsic disk luminosity $L_{\rm d} \approx 5 \times 10^{36} {\rm erg \, s^{-1}}$ for Sgr A* requires the disk to be inclined at $\theta_{\rm d} \gtrsim 87°$. Importantly, the constraint on $\theta_{\rm d}$ from this thin-disk model is not as stringent as that implied by a standard disk because a jet-modified disk is dimmer and redder as a result of efficient removal of accretion energy to power the jet. The disk luminosity and inclination are constrained by so far only a few

flux measurements in the NIR. Clearly, more NIR observations of Sgr A* in quiescence are needed to place tighter constraints on the steady-state disk spectrum (see also the discussion below on jet X-ray emission). Applications of this model to other more suitable LLAGN may thus provide better model constraints. So far, we have applied the model to M87 (Jolley & Kuncic 2007) and have found remarkably good agreement between the predicted and observed optical spectra, as well as the predicted jet power and that inferred from jet observations on kiloparsec scales. Furthermore, the model suggests that M87 may harbour a rapidly spinning black hole accreting at a rate of $10^{-3} M_\odot \, \mathrm{yr}^{-1}$.

We have not attempted here to model the X-ray emission from Sgr A*. However, Compton processes could be included in the jet spectral model to calculate the X-ray flux and further constrain the physical parameters by comparing with X-ray observations. By considering Compton scattering of the disk photons, in particular, we could in principle be able to indirectly constrain the intrinsic disk luminosity, L_{d}, and jet-modified spectrum. We note, however, that recent simultaneous NIR and X-ray observations of Sgr A* (Hornstein et al. 2007), revealing a constant spectral index during NIR flares and constant X-ray flux, may rule out inverse Compton emission by jet electrons off disk photons in favour of synchrotron self-comptonisation in the jet as the primary emission mechanism for the X-rays. The constancy of X-ray emission during NIR flares implies a separate source region for at least some of the NIR emission. In our model, emission shortward of 2μm is due primarily to disk emission and some of the uncorrelated flaring activity in this band could arise from stochastic magnetic reconnection events in the turbulent disk. On the other hand, NIR variability that is correlated with variability in the submm and/or X-ray bands (see e.g. Yusef-Zadeh et al. 2006) can arise in our model from prompt acceleration events in the jet that temporarily raise the high-energy cutoff in the electron energy distribution.

5. Conclusions

We have revisited theoretical constraints on thin-disk accretion in Sgr A*, showing that a geometrically-thick, hot, two-temperature accretion flow cannot be sustained in the presence of outflows and electron heating. We have revised observational constraints, taking into consideration modified disk emission as a result of magnetic coupling to a jet. The magnetic torque which drives the jet efficiently extracts accretion power from the disk at small radii. This results in an accretion disk that is dimmer than a standard relativistic disk accreting at the same rate, so the constraints on disk luminosity and inclination are less stringent. For Sgr A*, we infer a mass accretion rate of $\dot{M}_{\mathrm{a}} \simeq$ a few $\times 10^{-9} M_\odot \, \mathrm{yr}^{-1}$. We find that a disk luminosity of $L_{\mathrm{d}} \approx 5 \times 10^{36} \, \mathrm{erg \, s}^{-1}$ and an inclination angle $\gtrsim 87°$ are compatible with

existing observational constraints. However, more NIR observations of Sgr A* in quiesence are needed to provide tighter constraints on the presence of a cool accretion disk. Numerical simulations of radiative, low-$\dot{M}_a$ accretion flows are also warranted.

A.   Relativistic Disk Accretion

The relativistic theory for steady-state, geometrically-thin disk accretion onto a black hole was formulated by Novikov & Thorne (1973) and Page & Thorne (1974). In this formalism, the radiative disk flux can be conveniently expressed as the Newtonian solution derived by Shakura & Sunyaev (1973) multiplied by relativistic correction factors. Specifically, for a black hole with mass M and dimensionless spin parameter a, accreting at a rate $\dot{M}_a$, the radiative disk flux can be written as

$$F(x) = \frac{3}{8\pi} M^{-2} \dot{M}_a \, x^{-3} \, f^{\text{NT}}(x) \tag{A1}$$

where $r = Mx$ is the Boyer-Lindquist radial coordinate and $f^{\text{NT}}(x)$ is the Novikov–Thorne relativistic correction factor, defined by

$$f^{\text{NT}}(x) = \frac{A(x)}{C(x)} \quad , \quad \text{where} \quad C(x) \equiv 1 - 3x^{-1} + 2ax^{-3/2} \quad \text{and}$$

$$\begin{aligned} A(x) \equiv \; & 1 - \frac{y_{\text{ms}}}{y} - \frac{3a}{2y}\ln\left(\frac{y}{y_{\text{ms}}}\right) - \frac{3(y_1-a)^2}{yy_1(y_1-y_2)(y_1-y_3)}\ln\left(\frac{y-y_1}{y_{\text{ms}}-y_1}\right) \\ & - \frac{3(y_2-a)^2}{yy_2(y_2-y_1)(y_2-y_3)}\ln\left(\frac{y-y_2}{y_{\text{ms}}-y_2}\right) - \frac{3(y_3-a)^2}{yy_3(y_3-y_1)(y_3-y_2)}\ln\left(\frac{y-y_3}{y_{\text{ms}}-y_3}\right) \end{aligned} \tag{A2}$$

with $y = x^{1/2}$, $y_{\text{ms}} = x_{\text{ms}}^{1/2}$ and where

$$y_1 = 2\cos\left(\frac{1}{3}\cos^{-1}a - \frac{\pi}{3}\right) \quad , \quad y_2 = 2\cos\left(\frac{1}{3}\cos^{-1}a + \frac{\pi}{3}\right) \quad , \quad y_3 = -2\cos\left(\frac{1}{3}\cos^{-1}a\right) \tag{A3}$$

are the roots of the equation $y^3 - 3y + 2a = 0$. The last marginally stable orbit in the Kerr metric is given by:

$$x_{\text{ms}} = \left[3 + Z_2 - sign(a)\sqrt{(3-Z_1)(3+Z_1+2Z_2)}\right] \tag{A4}$$

where

$$Z_1 = 1 + (1 - a^2)^{1/3} \left[(1 + a)^{1/3} + (1 - a)^{1/3} \right] \qquad , \qquad Z_2 = \sqrt{3a^2 + Z_1^2} \qquad \text{(A5)}$$

A.1. Correction factor for a nonzero torque at the inner boundary

Agol & Krolik (2000) calculated a correction term for the radiative flux from a relativistic disk torqued at the inner boundary r_{ms}. In this case, the solution for the comoving disk flux can be generalized to

$$F(x) = \frac{3}{8\pi} M^{-2} \dot{M}_a x^{-3} \left[f^{\mathrm{NT}}(x) + f_{r\phi}^{\mathrm{nzt}}(x) \right] \qquad \text{(A6)}$$

The correction factor for the nonzero torque at x_{ms} is

$$f_{r\phi}^{\mathrm{nzt}}(x) = \frac{C_{\mathrm{ms}}^{1/2}}{C(x)} \frac{2\pi x_{\mathrm{ms}}^{5/2} T_{r\phi}(r_{\mathrm{ms}}) M \Omega_{\mathrm{ms}}}{x^{1/2} \dot{M}_a} \qquad \text{(A7)}$$

with $C_{\mathrm{ms}} = C(x_{\mathrm{ms}})$, $\Omega_{\mathrm{ms}} = \Omega(x_{\mathrm{ms}})$, where $\Omega = B^{-1} M^{-1} x^{-3/2}$ is the angular frequency of a circular orbit at radius r, with $B(x) = 1 + a x^{-3/2}$ and where

$$T_{r\phi}(r_{\mathrm{ms}}) = \int_{-h}^{+h} t_{r\phi}(r_{\mathrm{ms}}) \, \mathrm{d}z \qquad \text{(A8)}$$

is the vertically integrated radial-azimuthal magnetic stress at the last marginally stable orbit (see also Kuncic & Bicknell 2004).

A.2. Correction factor for a nonzero torque on the disk surface

Here we derive a correction term for the radiative flux of a relativistic disk with a nonzero magnetic torque on its surface. The disk is torqued by open field lines that do work against the surface. We identify this torque as being responsible for the formation of a magnetized corona and/or jet and we can write the generalized disk flux as

$$F(x) = \frac{3}{8\pi} M^{-2} \dot{M}_a x^{-3} \left[f^{\mathrm{NT}}(x) + f_{r\phi}^{\mathrm{nzt}}(x) - f_{\phi z}^{\mathrm{nzt}}(x) \right] \qquad \text{(A9)}$$

where $f_{\phi z}^{\mathrm{nzt}}(x)$ is the correction factor for the azimuthal-vertical magnetic stress that gives rise to a nonzero torque on the disk surface (Kuncic & Bicknell 2004).

We follow the procedure used by Page & Thorne (1974), using slightly different notation. We introduce the following parameters:

$$\xi = \frac{4\pi r F}{\dot{M}_\mathrm{a}} \quad , \quad \varpi = \frac{2\pi r T_\phi^{\,r}}{\dot{M}_\mathrm{a}} \quad , \quad \Upsilon = \frac{4\pi r t_\phi^{+z}}{\dot{M}_\mathrm{a}} \tag{A10}$$

where F is the disk flux measured in the fluid frame and t_ϕ^{+z} is the magnetic stress evaluated at the disk surface (Kuncic & Bicknell 2004).

Conservation of angular momentum can be expressed as

$$\left[L^\dagger - \varpi\right]_{,r} = \xi L^\dagger + \Upsilon \tag{A11}$$

where $L^\dagger$ is the specific angular momentum of a circular orbit at radius r. Energy conservation gives the relation $\varpi = BC^{1/2}\frac{\xi}{(-\Omega_{,r})}$ and substitution into (A11) then gives

$$\left[L^\dagger - BC^{1/2}\frac{\xi}{(-\Omega_{,r})}\right]_{,r} = \xi L^\dagger + \Upsilon \tag{A12}$$

This is a first-order differential equation in ξ with a general solution

$$\frac{C}{B^2(-\Omega_{,r})}\xi = \int_{r_\mathrm{ms}}^{r} \frac{C^{1/2}}{B}\left(L_{,r}^\dagger - \Upsilon\right)\,\mathrm{d}r + \frac{C_\mathrm{ms}}{B_\mathrm{ms}^2(-\Omega_{,r})_\mathrm{ms}}\xi_\mathrm{ms} \tag{A13}$$

The last term on the right hand side of this equation takes into account nonvanishing magnetic stresses at r_ms. Energy conservation and the expression for ϖ in (A10) give

$$\xi_\mathrm{ms} = \frac{B_\mathrm{ms}}{C_\mathrm{ms}^{1/2}}\frac{2\pi r_\mathrm{ms}T_\phi^{\,r}(r_\mathrm{ms})}{\dot{M}_\mathrm{a}}(\Omega_{,r})_\mathrm{ms} \tag{A14}$$

This term is set to zero in the Page & Thorne (1974) treatment.

The term in (A13) describing the effects of a nonzero suface torque is the one involving Υ. Using $(-\Omega)_{,r} = \frac{3}{2}B^{-2}M^{-2}x^{-5/2}$ with ξ and Υ (see (A10)), the comoving energy flux removed from the disk by this magnetic torque is

$$F_{\phi z}^\mathrm{nzt} = \frac{3}{8\pi}M^{-3}\dot{M}_\mathrm{a}x^{-7/2}C^{-1}\int_{r_\mathrm{ms}}^{r} \frac{C^{1/2}}{B}\frac{4\pi r t_\phi^{+z}}{\dot{M}_\mathrm{a}}\,\mathrm{d}r \tag{A15}$$

from which we deduce that the correction factor $f_{\phi z}^\mathrm{nzt}(x)$ for a nonzero torque on the surface of a relativistic disk, as defined in (A9), is

$$f_{\phi z}^\mathrm{nzt}(x) = M\dot{M}_\mathrm{a}^{-1}x^{-1/2}C^{-1}\int_{x_\mathrm{ms}}^{x} \frac{C^{1/2}}{B}4\pi x t_\phi^{+z}\,\mathrm{d}x \tag{A16}$$

REFERENCES

Agol E., 2000, ApJL, 538, L121

Agol E., Krolik J., 2000, ApJ, 528, 161

Aitken D., Greaves J., Chrysostomou A., Jenness T., Holland W., Hough J.H., Pierce-Price D., Richer J., 2000, ApJL, 534, L173

Balbus S. 2003, ARAA, 41, 555

Balbus S., Hawley J., 1991, ApJ, 376, 214

Becklin E. E., Gatley I., Werner M. W., 1982, ApJ, 258, 135

Begelman M. C., Chiueh T., 1988, ApJ, 332, 872

Beloborodov A., Levin Y., Eisenhauer F., Genzel R., Paumard T., Gillessen S., Ott T., 2006, ApJ, 648, 405

Bisnovatyi-Kogan G. S., Lovelace R. V. E., 2000, ApJ, 529, 978

Blackman E. G., 1999, MNRAS, 302, 723

Bower G. C., Wright M. C. H., Falcke H., Backer D. C., 2003, ApJ, 588, 331

Broderick A.E., Narayan R., 2006, ApJ, 638, L21

Cuadra J., Nayakshin S., Sunyaev R., 2003, A&A, 411, 405

Cuadra J., Nayakshin S., Springel V., Di Matteo T., 2006, MNRAS, 366, 358

Eisenhauer F., Schödel R., Genzel R., Ott T., Tecza M., Abuter R., Eckart A., Alexander T., 2003, ApJL, 597, L121

Falcke H., et. al., 1998, ApJ, 499, 731

Falcke H., Markoff S., 2000, A&A, 362, 113

Falcke H. 2001, Rev. Mod. Astron., 14, 31

Falcke, H., Körding, E., Markoff, S., 2004, A&A, 414, 895

Freeland, M. C., Kuncic, Z., Soria, R., Bicknell, G. V. 2006, MNRAS, 372, 630

Gallo, E. 2007, in "The Multicoloured Landscape of Compact Objects and their Explosive Origins", AIP Conf. Proc., in press (astro-ph/0702126)

Ghez A., Morris M., Becklin E., Tanner A., Kremenek T., 2000, Nature, 407, 307

Gruzinov A., 1998, ApJ, 501, 787

Hawley J., Balbus S., 2002, ApJ, 573, 738

Ho L., Filippenko A., Sargent W., 1997, ApJS, 112, 315

Hornstein, et al. 2007, ApJ, 667, 900

Ichimaru S., 1977, ApJ, 214, 840

Jolley E. J. D., Kuncic Z., 2007, ApSS, in press (astro-ph/0706.0763)

Kuncic Z., Bicknell G.V., 2004, ApJ, 616, 669

Kuncic Z., Bicknell G.V., 2007a, ApSS, in press (astro-ph/0705.0791)

Kuncic Z., Bicknell G.V., 2007b, Mod. Phys. Lett. A, in press (astro-ph/0707.1914)

Levin Y., Wu A., Thommes E., 2006, ApJ, 635, 341

Liu, B. F., Taam, R. E., Meyer-Hofmeister, E., Meyer, F. 2007, ApJ, in press (astro-ph/0709.0143)

Macquart J-P., Bower G. C., Wright M. C. H., Melvyn C. H., Backer D. C., Falcke H., 2006, ApJ, 646, L111

Maoz, D. 2007, MNRAS, in press (astro-ph/0702292)

Markoff S., Bower G. C., Falcke H., 2007, MNRAS, 379, 1519

Marrone D. P., Moran J. M., Zhao J.-H., Rao R., 2006, ApJ, 640, 308

Melia F., Liu S., Coker R., 2001, ApJ, 553, 146

Menten K. M., Reid M.J., Eckart A., Genzel R., 1997, ApJ, 475, L111

Merloni A., Fabian A.C., 2002, MNRAS, 332, 165

Merloni A., Heinz S., 2007, MNRAS, (in press, astro-ph/arXiv:0707.3356)

Miller J. M., Homan J., Miniutti G., 2006a, ApJ, 652, L113

Miller J. M., Homan J., Steeghs D., Rupen M., Hunstead R. W., Wijnands R., Charles P. A., Fabian A. C., 2006b, ApJ, 653, 525

Nagar, N. M., Wilson, A. S., Falcke, H. 2001, ApJ, 559, L87

Narayan R., Yi I., 1994, ApJ, 428, L13

Narayan R., Mahadevan R., Grindlay J., Popham R.G., Gammie C., 1998, ApJ, 492, 554

Novikov I. D., Thorne K. S., 1973, Black Holes, New York Gordon & Breach

Nayakshin S., Sunyaev, R. 2005, MNRAS, 364, L23

Nayakshin S., 2006, MNRAS, 372, 143

Nayakshin S., Dehnen W., Cuadra J., Genzel R., 2006, MNRAS, 366, 1410

Page D. N., Thorne K. S., 1974, ApJ, 191, 499

Paumard T., et al., 2006, ApJ, 643, 1011

Quataert E. 1998, ApJ, 500, 978

Quataert E., Gruzinov A., 1999, ApJ, 520, 248

Quataert E., Narayan R., 1999, ApJ, 520, 298

Quataert E., Gruzinov A., 2000, ApJ, 545, 842

Rees M. J., Phinney E. S., Begelman M. C., Blandford R. D., 1982, Nature, 295, 17

Rybicki G. B., Lightman A. P., 1979, Radiative Processes in Astrophysics, John Wiley & Sons, p. 173

Rykoff, E. S., Miller, J. M., Seeghs, D., Torres, M. A. P. 2007, ApJ, 666, 1129

Sano, T., Inutsuka, S. 2001, ApJ, 561, L179

Schödel R., et al., 2002, Nature, 419, 694

Shakura N. I., Sunyaev R. A., 1973, A&A, 24, 337

Shapiro S. L., Lightman A. P., Eardley D. M., 1976, ApJ, 204, 197

Sharma P., Quataert E., Hammett G., Stone J., 2007, ApJ, 667, 714 (astro-ph/0703572)

Shen Z. Q., Lo K. Y., Liang M. C., Ho P. T. P., Zhao J.-H., 2005, Nature, 438, 62

Trippe S., Paumard T., Ott T., Gillessen S., Eisenhauer F., Martins F., Genzel R., 2007, MNRAS, 375, 764

Yuan F., Markoff S., Falcke H., 2002, A&A, 383, 854.

Yuan F., Quataert E., Narayan R., 2003, ApJ, 598, 301 598, 301.

Yuan F., Quataert E., Narayan R., 2004, ApJ, 606, 894

Yuan, F. 2006, J. Phys. Conf. Ser., 54(1), 427 (astrop-ph/0607123)

Yusef-Zadeh, F., et al. 2006, ApJ, 644, 198.

––